Supplementary Information (SI) for Journal of Materials Chemistry A.
This journal is © The Royal Society of Chemistry 2024

Supplementary Information

High Power Metal-Support Protonic Ceramic Fuel Cell using Increased Proton Conductivity in Cathode Functional Layer of $La_{1-x}Sr_xScO_3$ (LSSc, x=0.1-0.25)

Hyo-Young Kim [a], Motonori Watanabe [ab], Jun Tae Song [bc], Miki Inada [bc] and Tatsumi Ishihara *[abc]

a Department of Automotive Science, Graduate School of Integrated Frontier Sciences, Kyushu University, Motooka 744, Nishiku, Fukuoka, 819-0395, Japan
[b] International Institute for Carbon Neutral Energy Research (WPI-I^{2}CNER), Kyushu University, Motooka 744, Nishiku, Fukuoka, 819-0395, Japan
[c] Department of Applied Chemistry, Faculty of Engineering, Kyushu University, Motooka 744, Nishiku, Fukuoka, 819-0395, Japan
*Corresponding author email: ishihara@cstf.kyushu-u.ac.jp

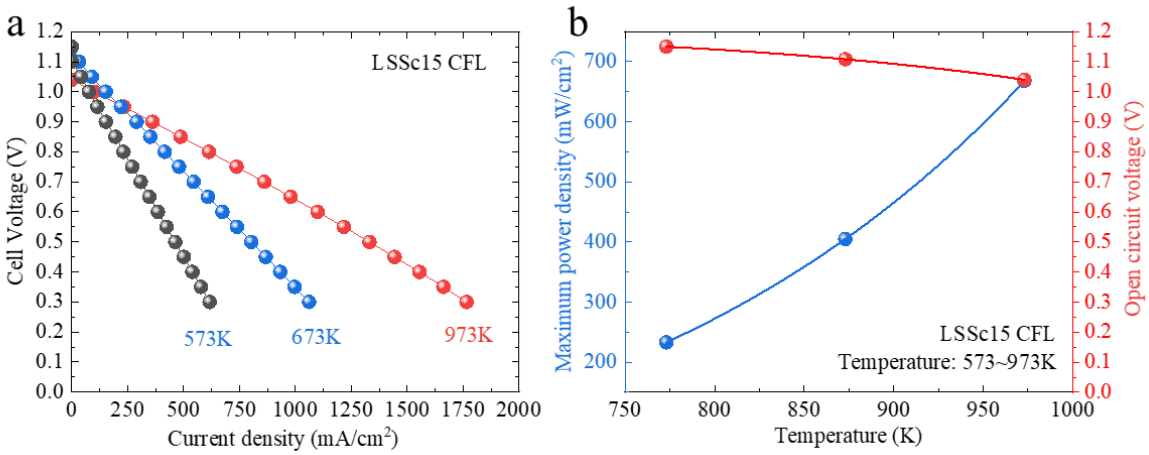

Figure S1. I-V curve and temperature dependence of MPD and OCV of the cell using LSSc15 CFL

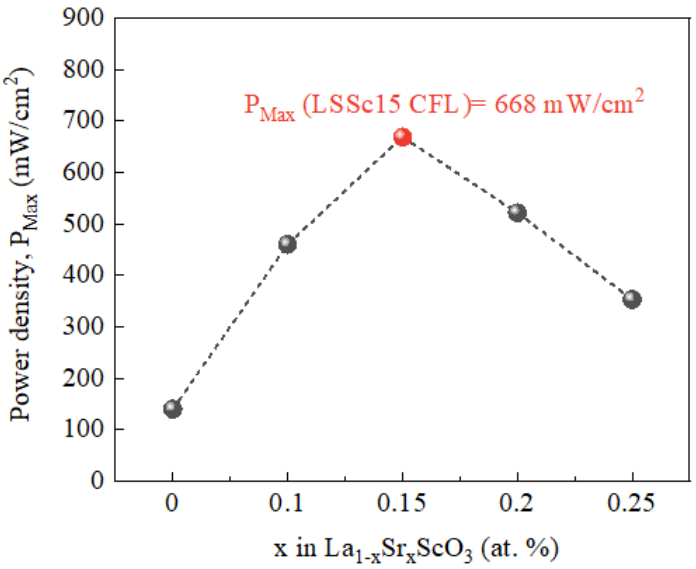

Figure S2. Comparison of maximum power density with different Sr dopant

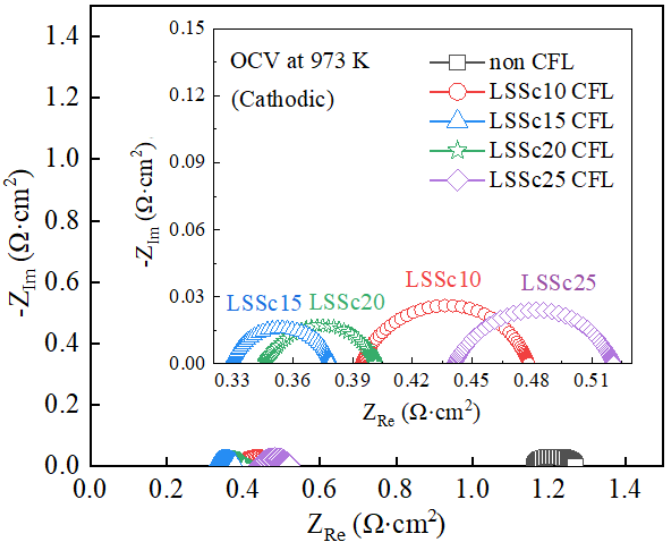

Figure S3. EIS spectra of cathodic non, LSSc10, LSSc20, and LSSc25 CFL at 973K.

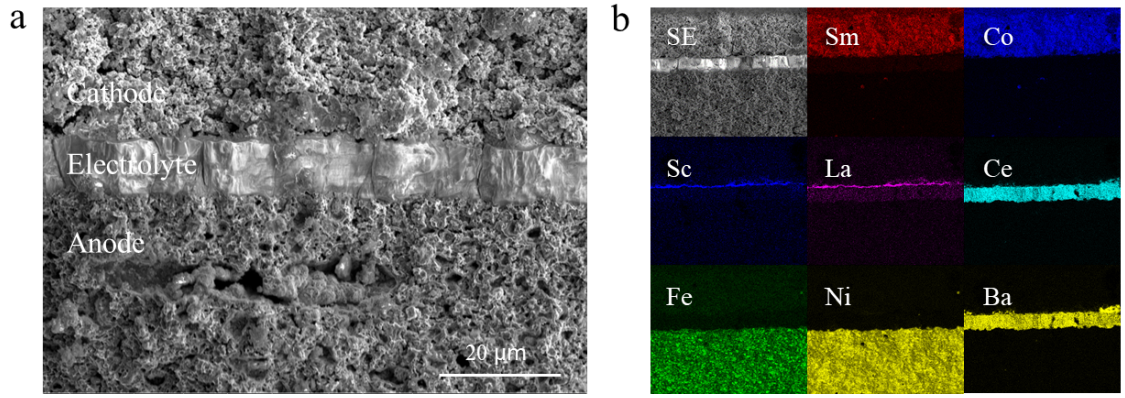

Figure S4. (a) SEM and (b) EDS-mapping image of the cross-section after cell test.

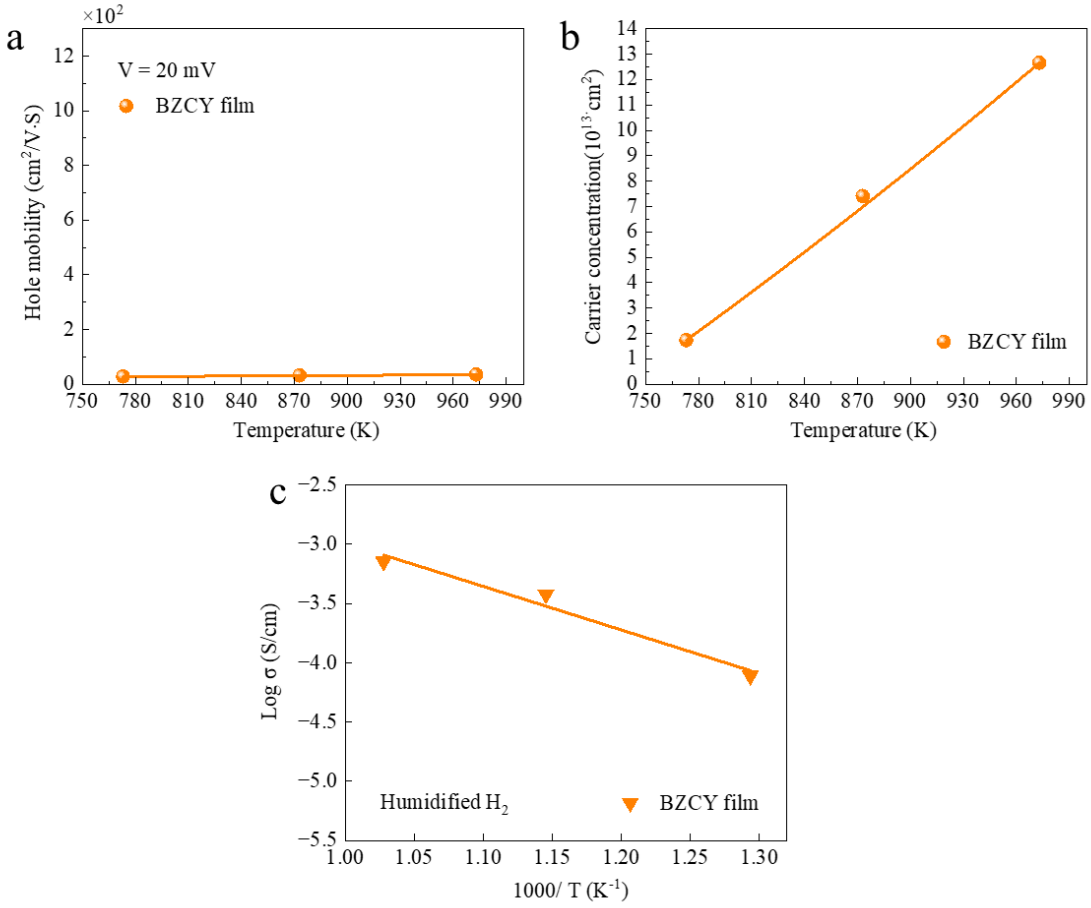

Figure S5. (a) Hole mobility (b) carrier concentration (c) conductivity of BZCY film under humidified (3% H_2O) H_2 condition.

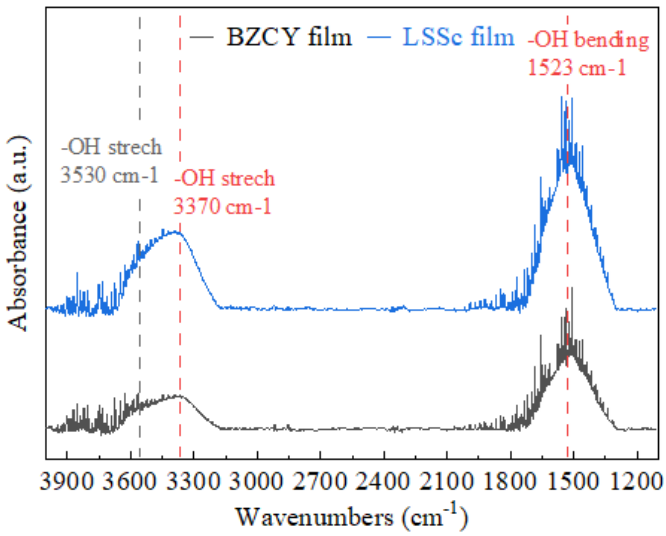

Figure S6. FT-IR spectra of LSSc and BZCY film after exposure to humidified condition at room temperature.

FT-IR spectroscopy was conducted to assess the proton concentration of LSSc and BZCY films by analyzing the amount of hydroxyl (OH) group in the film. As shown in **Figure S4**, the FT-IR spectra reveal two strong but broad absorption bands at approximately 3530 and 3370 cm^{-1}. The peak at 3530 cm^{-1} is typically attributed to OH bands associated with adsorption of water. The stronger intensity of the OH band suggests that the proton concentration in the LSSc was larger than that of BZCY. Compared to BZCY, LSSc shows an increased intensity of the 3370 cm^{-1} peak, suggesting a higher proton concentration in LSSc films. In particular, the strong OH peak around 1523 cm^{-1} also indicates water adsorption or hydration in proton-conducting materials, so these results can support high proton concentration in LSSc film.

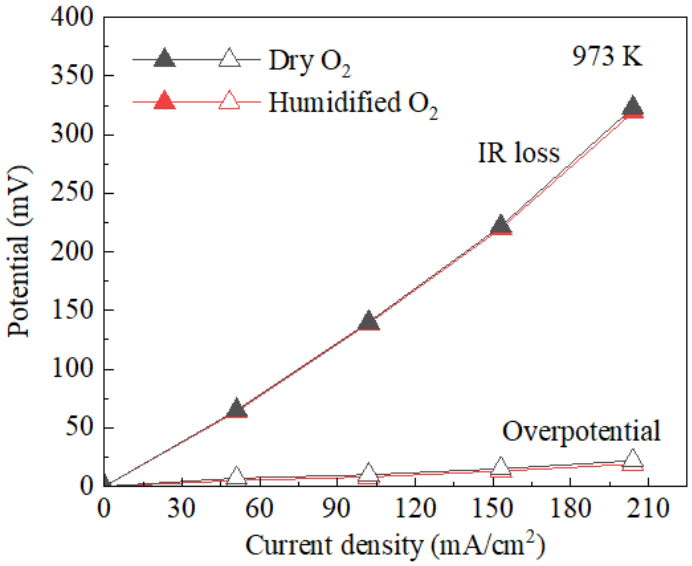

Figure S7. Internal resistance of dry and humidified O_2 without CFL

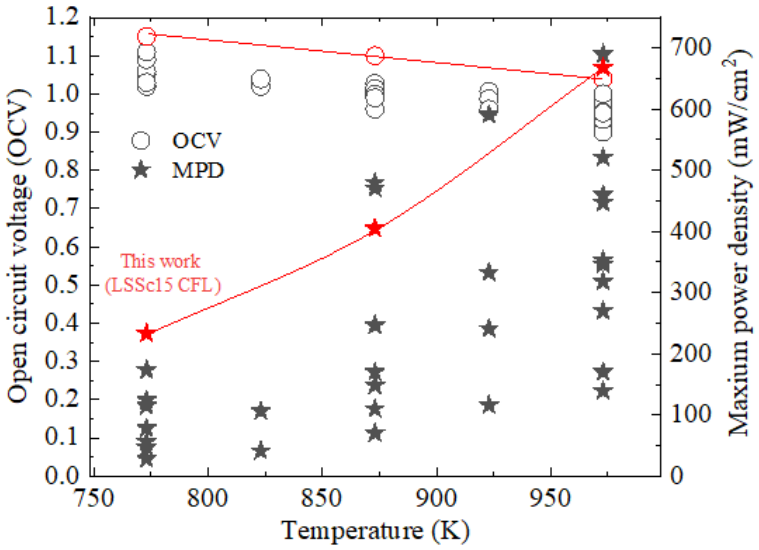

Figure S8. Comparison of OCV and MPD with conventional PCFCs as shown in Table S3 and proposed cell (LSSc CFL)

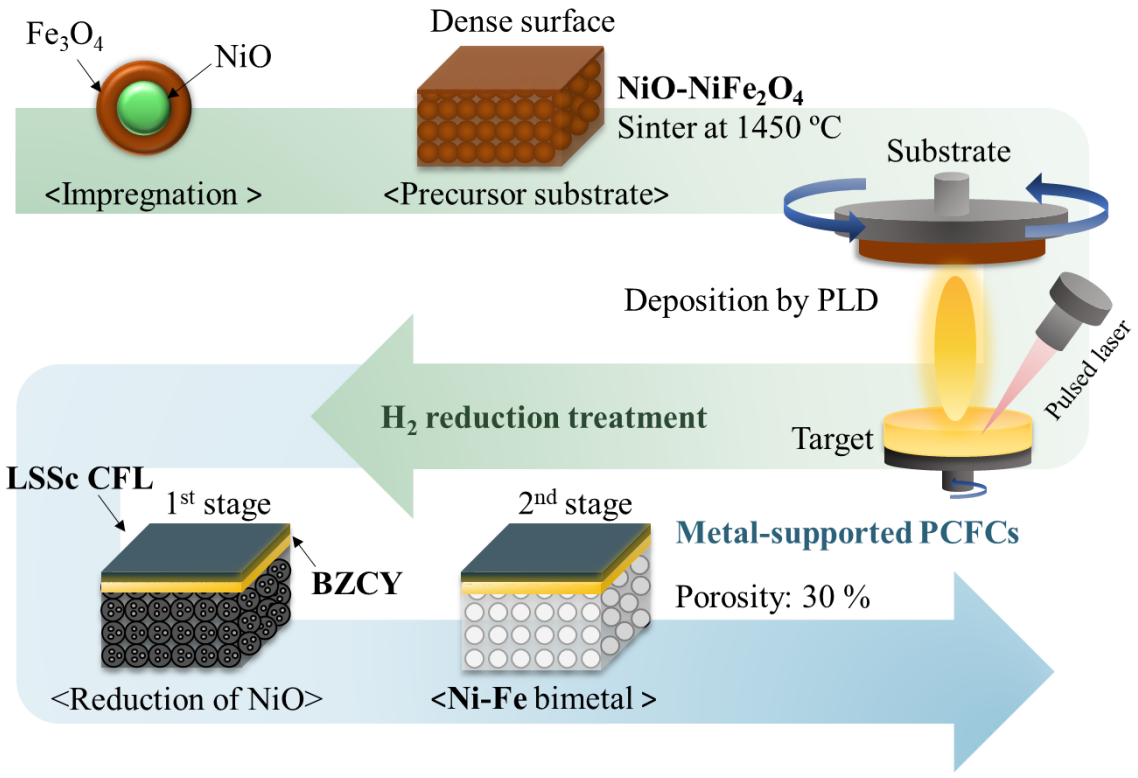

Figure S9. Schematic image of PCFCs preparation

Table S1. Element composition of LSSc20 bulk and film

at % (wt %)	Bulk	Film
La	36.58 (0.73)	36.32 (0.73)
Sr	8.90(0.18)	8.34 (0.17)
Sc	54.52 (1.1)	55.33 (1.11)

Table S2. Comparison of anode support before and after the reaction

Reduction	Diameter	Porosity	Shrinkage
Before (NiO-$NiFe_2O_4$)	18.5 mm	0.05 %	5.5 % by dilatometer
After (Ni-Fe)	17.5 mm	30.1 %	

Table S3. Cell performances of PCFCs with LSSc CFL measured in this study at 973K

No.	Support	Electrolyte	Interlayer	Cathode	OCV (V)	MPD (mW/cm^2)	Ohmic ($\Omega \cdot cm^2$)	Polarization ($\Omega \cdot cm^2$)
1	Porous Ni-Fe	$BaZr(Ce,Y)O_3$	BZCY	$Sm_{0.5}Sr_{0.5}CoO_3$	0.95	139	1.15	0.11
2	Porous Ni-Fe	$BaZr(Ce,Y)O_3$	LSS10	$Sm_{0.5}Sr_{0.5}CoO_3$	1.0	460	0.39	0.08
3	Porous Ni-Fe	$BaZr(Ce,Y)O_3$	LSS15	$Sm_{0.5}Sr_{0.5}CoO_3$	1.04	668	0.32	0.05
4	Porous Ni-Fe	$BaZr(Ce,Y)O_3$	LSS20	$Sm_{0.5}Sr_{0.5}CoO_3$	1.0	521	0.34	0.06
5	Porous Ni-Fe	$BaZr(Ce,Y)O_3$	LSS25	$Sm_{0.5}Sr_{0.5}CoO_3$	1.0	353	0.44	0.08

Table S4. Comparison of conventional PCFCs using BZCY electrolyte

Author (Years)	Electrolyte	Anode Support	Oeprating Temperature (K)	Open Circuit Voltage (V)	Power Density (mW/cm^2)	Ref.
Wang et al. (2006)	BZCY	Ni-BZCY	973	0.97	270	[1]
			873	1.01	148	
			773	1.05	56	
Peng et al. (2024)	BZCY	Ni-BZCY	973	0.975	690	[2]
			923	1.007	591	
			873	1.027	471	
Ma et al. (2021)	BZCY	Ni-BZCY	973	0.92	318	[3]
			923	0.96	241	
			873	1.0	170	
			823	1.02	106	
Bae et al. (2015)	BZY	Ni-BZY	973	0.9	346	[4]
			873	0.96	246	
			773	1.05	115	
Pergolesi et al. (2010)	BZY	Ni-BZY	873	0.99	110	[5]
			773	1.06	47	
Sun et al. (2010)	BZY	Ni-BZY	973	0.953	170	[6]
			923	0.987	116	
			873	1.014	70	
			823	1.039	41	
Duan et al. (2015)	BZY	Ni-BZY	873	1.0	480	[7]
Qian et al. (2014)	BZY/BCY	Ni-BZCY	973	0.933	447	[8]
			923	0.96	333	
			873	0.99	247	
			773	1.02	173	

Reference of Supporting Information

1. B. Wang, L. Bi, and X. S. Zhao, *J. Power Sources*, 2018, **399**, 207-214.
2. C. Peng, B. Zhao, X. Meng, X. Ye and T. Luo, *Membranes*, 2024, **14**, 61.
3. Y. Ma, J. Huang and B. He, *Ceram. Int.*, 2021, **47**, 14680-14688.
4. H. Bae and G.M. Choi, *J. Power Sources*, 2015, **285**, 431-438.
5. D. Pergolesi, E. Fabbri and E. Traversa, *Electrochem. Commun.*, 2010, **12**, 977-980.
6. W. Sun., L. Yan, Z. Shi, Z. Zhu and W. Liu, *J. Power Sources*, 2010, **195**, 4727-4730.
7. C. Duan, J. Tong, M. Shang, S. Nikodemski, M. Sanders, S. Ricote, A. Almansoori and R. O'hayre, *Science*, 2015, **349**, 1321-1326.
8. J. Qian, W. Sun, Q. Zhang, G. Jiang and W. Liu, *J. Power Sources*, 2014, **249**, 131-136.